Mon. Not. R. Astron. Soc. **000**, 000–000 (0000) Printed 23 July 1997 (MN LATEX style file v1.4)

New diameter measurements for 10 Mira variables: Implications for effective temperatures, atmospheric structure and pulsation modes

C.A. Haniff,[1] M. Scholz[2] and P.G. Tuthill[1⋆]
[1] *Mullard Radio Astronomy Observatory, Cavendish Laboratory, Madingley Road, Cambridge CB3 0HE*
[2] *Institut für Theoretische Astrophysik der Universität Heidelberg, Im Neuenheimer Feld 561, D-69120 Heidelberg, Germany*

Accepted 1995 May 5. Received 1994 April 4; in original form 1994 December 7

ABSTRACT
We present new and precise multi-wavelength angular diameter measurements for 10 long-period variables. After correction for limb-darkening and photospheric extension, we use these to investigate the effective temperatures, physical diameters and pulsation modes of the stars. For all 10 stars in the sample, our measurements imply photospheric radii in excess of 350 $R_{\odot}$, thereby supporting the recent result of Tuthill et al. Unless the favoured mass scale for Miras is increased by at least a factor of two, or our current understanding of their period–luminosity relation is incorrect, our data provide strong evidence against fundamental-mode pulsation in Mira variables with periods in the range 280 – 430 d.

Key words: stars: fundamental parameters – stars: late-type – stars: oscillations.

1 INTRODUCTION

Developments in detector technology and image processing methods have now made interferometric imaging with large ground-based telescopes relatively straightforward, at least for bright astrophysical sources – see e.g. Roddier (1988) for a review. Such interferometric methods now permit measurement of the complex visibility function of the source (i.e. the Fourier transform of the brightness distribution) which can be inverted to provide true diffraction-limited images. The spatial resolutions thus attainable are typically tens of milli-arcseconds using existing 4-m class telescopes. As a consequence these methods have been usefully exploited in a number of studies of cool evolved stars for which structures on scales comparable to that of the stellar disc have been investigated (Buscher et al. 1990; Haniff et al. 1992; Wilson et al. 1992).

As part of a continuing programme of optical interferometric imaging we have used variants of the non-redundant mask (NRM) method (Haniff et al. 1987; Nakajima et al. 1989; Haniff & Buscher 1992) to study a sample of 10 nearby long-period variable stars. Despite much observational work (see e.g. Habing 1990) many fundamental aspects of Mira variables remain unclear. These include their detailed atmospheric structure (see e.g. Beach, Willson & Bowen 1988 and Bessell et al. 1989 for two differing viewpoints), their effective temperature scale (Bessell et al. 1989) and their mode of pulsation (Wood 1990a,b). Many authors have noted the potential of accurate monochromatic diameter measurements for addressing a number of these issues (Labeyrie et al. 1977; Bonneau et al. 1982; Scholz & Takeda 1987; Bessell et al. 1989). However, previous efforts in this area have been hampered by the large uncertainties associated with converting apparent angular diameter measurements to more physically meaningful photospheric diameters. Fortunately, the advent of detailed numerical modelling of Mira atmospheres (Bessell et al. 1989; Bessell & Scholz 1989; Scholz 1992; Bessell, Scholz & Wood 1995, hereafter BSW) has gone some way towards resolving this problem.

Recently Tuthill et al. (1994a) have exploited these models in a study of the long-period variable R Leonis. By combining interferometric angular diameter measurements at selected wavelengths with recent model photospheres and a reliable distance estimate, Tuthill et al. were able to derive accurate estimates for both the effective temperature and the photospheric radius of the star. Their data argue strongly against the hypothesis of fundamental-mode pulsation in R Leonis, but only add further to the current controversy surrounding mode identification in long-period variables. A number of studies based on photometry and empirically determined period–luminosity relations have sug-

⋆ Current address: Space Sciences Laboratory, University of California at Berkeley, Berkeley, California 94720, USA.

gested first-overtone pulsation (Wood 1975; Robertson & Feast 1981; Glass & Feast 1982), yet the dynamical behaviour of Mira variables, as measured via CO velocities, is most satisfactorily explained assuming fundamental-mode pulsation (Hill & Willson 1979; Willson 1983). However, even these dynamical studies have proven contentious, with Tuchman (1991) drawing somewhat different conclusions using the same observational data.

In an effort to establish the wider validity of the result of Tuthill et al. (1994a) we present here new interferometric measurements of 10 nearby Mira variables, including R Leonis. To facilitate comparison with results in the literature we present estimates of the angular diameter of each star derived from fitting circularly symmetric uniform-disc and Gaussian models to measured visibility functions. We compare our data with the predictions of model atmosphere calculations in order to reduce our monochromatic diameter estimates to a set that more closely represents the continuum photospheric diameter. Furthermore, we assess the extent to which these theoretical models can successfully reproduce the intensity profiles across the stars and their variation as a function of wavelength. By combining our photospheric diameters with near-infrared photometry and distance estimates for each star, we have investigated the effective temperatures and possible pulsation modes of the sample members.

2 OBSERVATIONS AND DATA REDUCTION

Interferometric data were obtained at the Ground-based High Resolution Imaging Laboratory (GHRIL) of the William Herschel Telescope (WHT) during five separate observing runs over the period 1992 January – 1993 December. At each epoch, suitable targets were selected on the basis of their apparent brightness and position on the sky. The sample is thus in no way statistically complete, and is biased towards bright, and therefore nearby, Miras.

Although some minor details of the observing setup and data collection varied between observing runs (e.g. the precise pixel scales and exposure times), the basic procedures were broadly similar to those used in previous high-resolution imaging experiments (Buscher et al. 1990; Wilson et al. 1992). An achromat placed beyond the nominal Nasmyth focus was used to provide a collimated beam which was masked with an aperture in the pupil plane and then re-imaged, at high magnification, on to a CCD. A variety of mask geometries were employed including four- and five-hole non-redundant designs, and, in cases where the source was particularly faint, a narrow slit. Wavelength selection was provided by one of four interference filters centred on 700, 710, 833 or 902 nm. These had bandwidths (FWHM) of 10, 10, 41 and 50 nm respectively. For our sample of late-type stars, the 710-nm filter is situated in a region of the spectrum with a strong molecular absorption feature due to TiO, whilst the other filters isolate continuum windows contaminated to a greater or lesser extent with atomic and molecular absorption features. As in our previous experiments, no atmospheric dispersion correction was employed due to the small zenith distances, relatively narrow bandwidths, and long central wavelengths at which the sources were observed. For each observation, between 15 000 and 25 000 short-exposure images of each source were secured, using exposure times in the range 7 – 10 ms. Further details of the observations are given in Table 1.

Visibility amplitudes and bispectrum phases were recovered from the data following standard methods (Haniff et al. 1987; Buscher et al. 1990), and were calibrated using identical observations of known unresolved stars. At each epoch, observations of close binary stars with well-known orbits (Hartkopf, personal communication) were made to determine the plate scale and orientation of the detector, and to assess the fidelity of the data analysis. The errors in the scale and orientation of our final images were estimated to be 1.5 per cent and $0.^\circ5$ respectively.

3 RESULTS

The interpretation of visibility amplitude data has, in the past, often been seen to be one of the most unreliable aspects in the analysis of interferometric observations of Mira variables. Although it is customary to fit simple circularly symmetric uniform-disc models to the data, it is now well established that the brightness distributions of Miras are unlikely either to be uniform (Scholz & Takeda 1987) or to exhibit circular symmetry (Karovska, Nisenson & Papaliolios 1991; Haniff et al. 1992; Quirrenbach et al. 1992; Wilson et al. 1992; Tuthill, Haniff & Baldwin 1994b).

In the following subsections we present two analyses of our visibility data. In the first case, we have utilized simple uniform-disc and Gaussian functions to enable a comparison to be made with results in the literature, whereas in the second we have used a set of recent model photospheres to estimate the effects of limb-darkening, photospheric extension and variability on our data. In the latter instance we have further improved on earlier studies by explicitly accounting for any peculiarities in the brightness distributions across the stars, and by not assuming circular symmetry.

3.1 Fitting of simple models

Preliminary estimates of the angular diameters of the stars in the sample were obtained by fitting either uniform-disc or circularly symmetric Gaussian models to the calibrated visibility amplitudes. In parallel, the data were also inspected for evidence of departures from circular symmetry. Following Tuthill et al. (1994a), this was assessed via a three-stage procedure. First, the Fourier data were inverted to produce diffraction-limited images of each source, which were then examined. A second step involved the inspection of the Fourier data – the presence of non-zero bispectrum phases or modulations of visibility amplitude with position angle on the sky were taken to be indicative of departures from circular symmetry. Finally, attempts were made to fit more complicated models to the visibilities to assess to what extent more complex brightness distributions could better fit the measured data.

In general the sources fell into two distinct categories. The first of these comprised those sources that were only

Table 1. Best-fitting one-parameter models for the LPV sample. Filter wavelengths are measured in nm. The timings of the observations are identified by the calendar date of the night of the observation. Periods are from Kholopov (1987) and pulsation phases have been determined from AAVSO records (Mattei, private communication). For the uniform-disc (UD) fits the diameter is given, whereas for Gaussian models the full width at half maximum is quoted. 1σ errors are shown. For further details see the text.

Object & period (d)	Date (d/m/y)	Variability phase	Filter $\lambda/\Delta\lambda$	UD (mas)	Gaussian (mas)
o Cet	18/01/92	0.58	700/10	44.6 ± 3.0	30.1 ± 2.0
332	18/01/92	0.58	710/10	53.0 ± 4.5	35.6 ± 3.2
	18/01/92	0.58	902/50	37.9 ± 3.5	23.3 ± 2.0
	11/07/92	0.05	700/10	39.4 ± 3.4	26.4 ± 3.4
	13/07/92	0.05	700/10	42.0 ± 3.2	28.3 ± 2.2
	13/07/92	0.05	710/10	45.8 ± 4.7	31.7 ± 3.0
	11/07/92	0.05	833/41	44.0 ± 5.3	29.6 ± 3.6
	13/07/92	0.05	833/41	40.7 ± 4.4	26.3 ± 3.1
	12/07/92	0.05	902/50	36.4 ± 2.0	22.7 ± 1.2
	03/01/93	0.48	700/10	43.4 ± 3.0	27.6 ± 1.8
	04/01/93	0.48	902/50	37.2 ± 3.2	23.0 ± 2.0
U Ori	06/12/93	0.04	700/10	28.1 ± 2.0	17.3 ± 1.2
368	07/12/93	0.04	833/41	22.9 ± 3.0	13.8 ± 2.0
R Cnc	02/01/93	0.14	700/10	31.6 ± 3.4	19.8 ± 2.1
362	03/01/93	0.14	902/50	22.5 ± 4.0	13.9 ± 3.0
R Leo	20/01/92	0.27	833/41	44.9 ± 2.0	28.8 ± 1.5
310	20/01/92	0.27	902/50	43.3 ± 2.0	27.8 ± 1.5
	10/06/93	0.88	700/10	64.2 ± 5.7	40.8 ± 2.5
	10/06/93	0.88	710/10	67.9 ± 7.0	45.8 ± 4.0
R Hya	07/06/93	0.28	700/10	37.2 ± 3.3	23.4 ± 2.0
389	09/06/93	0.28	833/41	36.0 ± 4.0	22.7 ± 2.5
	08/06/93	0.28	902/50	34.1 ± 3.4	20.9 ± 2.2
W Hya	08/06/93	0.04	700/10	65.9 ± 4.8	46.0 ± 3.4
361	09/06/93	0.04	700/10	64.7 ± 5.2	46.7 ± 3.8
	09/06/93	0.04	710/10	79.5 ± 3.6	53.6 ± 2.4
R Aql	11/07/92	0.06	700/10	24.6 ± 6.0	15.0 ± 4.0
284	12/07/92	0.06	710/10	30.4 ± 4.0	21.2 ± 3.0
χ Cyg	13/07/92	0.32	700/10	39.5 ± 4.0	24.4 ± 2.5
408	13/07/92	0.32	833/41	33.3 ± 4.0	20.7 ± 3.0
	13/07/92	0.32	902/50	32.9 ± 2.0	19.6 ± 1.5
	07/06/93	0.14	700/10	34.0 ± 1.6	21.4 ± 1.0
	08/06/93	0.14	710/10	41.2 ± 4.0	27.9 ± 2.5
	07/09/93	0.35	700/10	43.5 ± 4.0	26.4 ± 2.5
T Cep	12/07/92	0.72	700/10	33.9 ± 4.0	21.8 ± 2.6
388	12/07/92	0.72	902/50	27.4 ± 6.0	20.0 ± 5.0
	07/06/93	0.56	833/41	29.0 ± 4.0	18.6 ± 2.5
R Cas	13/07/92	0.05	700/10	41.4 ± 4.0	26.8 ± 2.5
430	13/07/92	0.05	700/10	42.9 ± 5.0	28.0 ± 3.2
	13/07/92	0.05	710/10	51.0 ± 5.0	36.1 ± 3.4
	13/07/92	0.05	710/10	55.5 ± 5.0	36.4 ± 3.4
	13/07/92	0.05	833/41	30.8 ± 3.0	18.9 ± 2.0
	08/06/93	0.82	700/10	42.5 ± 4.0	27.3 ± 3.0
	07/09/93	0.03	700/10	41.2 ± 2.5	26.7 ± 1.6
	08/09/93	0.03	710/10	54.1 ± 3.4	34.4 ± 2.2
	08/09/93	0.03	833/41	33.0 ± 4.0	20.3 ± 2.5

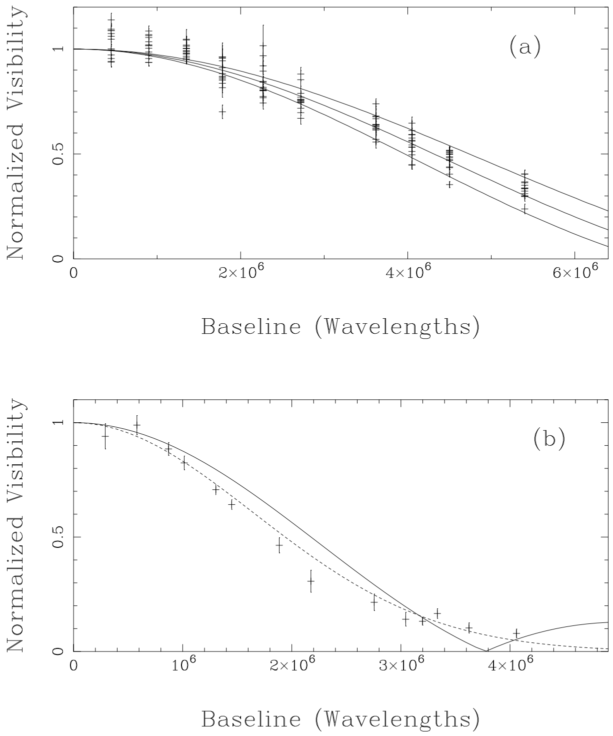

Figure 1. Normalized visibility amplitudes for χ Cyg at 700 nm (a) and R Leo at 710 nm (b). In both cases the data are from 1993 June. In the first panel (a) the data are shown with visibility curves for three uniform-disc models of diameter 30.7, 33.7, and 36.7 mas. In the second panel (b) an azimuthally averaged dataset has been plotted together with Gaussian (dotted line) and uniform-disc (full line) model visibility curves.

marginally resolved (U Ori, R Cnc, R Hya, R Aql, and T Cep) and which could be adequately characterized with simple circularly symmetric models. The remaining sources were more fully resolved and their visibility data were indicative of more complex morphologies. Models that incorporated a small number (either one or two) of bright unresolved features superimposed on a circularly symmetric disc often provided good fits to the data (o Ceti, R Leo, χ Cyg, and R Cas), though for one source (W Hya) an elliptical disc model also proved satisfactory. Apart from the case of o Ceti, the diameters inferred from these more complicated models differed by no more than ~ 15 per cent from those obtained with the simpler analysis. For o Ceti, estimates of the stellar diameter obtained using the more complicated model-fitting procedure were up to 50 per cent larger (at 700 and 710 nm) than those derived using one-component models. In order to permit comparison with measurements in the literature, for this first-pass analysis, any deviations from circular symmetry were ignored, and the diameters presented in Table 1 were obtained by fitting circularly symmetric models to the visibility amplitudes alone. Because of the systematic trends noted when fitting more complex models, the reader should be aware that for those sources known to have asymmetric brightness distributions the figures in Table 1 represent lower limits.

Results for a typical dataset are presented in Fig. 1(a) which shows three uniform-disc model visibility curves overplotted on a full set of visibility amplitude measurements for χ Cyg. Although in this case the median diameter model fits the data adequately, for stars that were highly resolved, the nulls and secondary maxima expected for a uniformly bright and hard-edged disc were not seen. Fig. 1(b) shows an example of this for the star R Leo. Here we have plotted the azimuthally averaged visibility amplitude together with a uniform-disc and a Gaussian model. At long baselines the uniform-disc model cannot reproduce the gradual flattening-off of the visibility curve, and so using such a model to parametrize the star would be likely to lead to systematic errors. In order to avoid this difficulty we have chosen to present fitted diameters for both uniform-disc and Gaussian models in Table 1. Sources for which the visibility function had not fallen below $\sim$ 15 per cent at the longest baseline measured could be satisfactorily described by either type of model; more resolved sources were likely to be better quantified by the Gaussian FWHM. For both types of models, 1σ errors were estimated from the sum of the squared differences between the models and data. The reader should note that these errors do not include systematic effects arising from, for example, apparent ellipticities of the stellar brightness distribution.

3.2 Photospheric angular diameters

While being convenient for parametrizing the extent of any particular star, the raw 'diameters' presented in Table 1 are only of limited value. To be of use in an astrophysical context it was necessary to convert these measures into estimates of the 'true' photospheric size. For cool variable stars, such as those in our sample, such a procedure has to accommodate the variation of diameter both with pulsation phase (or even cycle) and with the strongly wavelength-dependent opacity in the outer stellar atmosphere (Scholz & Takeda 1987; Bessell et al. 1989; Scholz 1993; BSW). Indeed, for stars with extended atmospheres even the notion of a photospheric diameter can lead to problems, there being a number of competing definitions (Baschek, Scholz & Wehrse 1991). In this paper we have followed Ridgway et al. (1992) and Tuthill et al. (1994a) and adopted the conventional definition in which the photospheric radius R is an optical-depth radius given by the distance from the star's centre at which the Rosseland optical depth equals unity. This radius has the advantage of agreeing closely with measurable near-infrared continuum radii and with the standard boundary radius of pulsation models that enters in calculations of, for example, the effective temperature $T_{\rm eff}$ and the pulsation constant Q. In the following sections effective temperatures will always refer to this Rosseland radius.

In order to account for the effects of limb-darkening, atmospheric extension and variability phase, we used a set of theoretical Mira models to predict the centre-to-limb surface brightness distributions expected at the wavelengths corresponding to the filters used during our observations. When using such models, previous authors (Ridgway et al.

Table 2. Photospheric diameters (referring to the layer of unit Rosseland optical depth) inferred by fitting theoretical centre-to-limb brightness profiles for Miras to our visibility data. The format of the table is similar to that of Table 1. The reader should note that, although each measurement is identified with a particular observing wavelength (column 4), the values given in columns 5 and 6 are estimates of the photospheric diameter as defined above. The D and E notation refers to fundamental and first-overtone models respectively. For further details see the text.

Object & period (d)	Date (d/m/y)	Variability phase	Filter $\lambda/\Delta\lambda$	D Model (mas)	E Model (mas)
o Cet	18/01/92	0.58	700/10	40.6 ± 5.8	36.5 ± 3.2
332	18/01/92	0.58	710/10	47.1 ± 6.7	42.0 ± 4.2
	18/01/92	0.58	902/50	37.4 ± 4.3	32.6 ± 3.4
	11/07/92	0.05	700/10	34.8 ± 5.2	31.2 ± 3.2
	13/07/92	0.05	700/10	37.4 ± 5.4	33.6 ± 3.2
	13/07/92	0.05	710/10	43.5 ± 6.9	38.9 ± 4.5
	11/07/92	0.05	833/41	42.3 ± 6.7	36.3 ± 4.7
	13/07/92	0.05	833/41	39.5 ± 6.1	34.0 ± 4.0
	12/07/92	0.05	902/50	36.4 ± 3.1	31.7 ± 2.4
	03/01/93	0.48	700/10	37.8 ± 5.3	33.9 ± 3.1
	04/01/93	0.48	902/50	38.6 ± 4.2	33.7 ± 3.4
U Ori	06/12/93	0.04	700/10	24.7 ± 3.5	22.2 ± 2.0
368	07/12/93	0.04	833/41	21.3 ± 3.7	18.5 ± 2.6
R Cnc	02/01/93	0.14	700/10	27.7 ± 4.5	24.9 ± 3.0
362	03/01/93	0.14	902/50	19.7 ± 3.8	17.9 ± 3.6
R Leo	20/01/92	0.27	833/41	43.0 ± 4.9	36.9 ± 2.4
310	20/01/92	0.27	902/50	43.6 ± 3.3	38.0 ± 2.6
	10/06/93	0.88	700/10	55.6 ± 8.3	49.7 ± 5.2
	10/06/93	0.88	710/10	60.9 ± 9.4	53.9 ± 6.3
R Hya	07/06/93	0.28	700/10	32.7 ± 4.9	29.4 ± 3.1
389	09/06/93	0.28	833/41	33.2 ± 5.2	28.7 ± 3.5
	08/06/93	0.28	902/50	32.9 ± 3.9	28.7 ± 3.2
W Hya	08/06/93	0.04	700/10	58.6 ± 8.3	52.4 ± 4.9
361	09/06/93	0.04	700/10	60.9 ± 8.8	54.4 ± 5.4
	09/06/93	0.04	710/10	71.4 ± 9.2	63.9 ± 4.5
R Aql	11/07/92	0.06	700/10	24.0 ± 6.6	21.5 ± 5.4
284	12/07/92	0.06	710/10	26.0 ± 4.6	23.3 ± 3.2
χ Cyg	13/07/92	0.32	700/10	34.2 ± 5.4	30.7 ± 3.6
408	13/07/92	0.32	833/41	34.5 ± 5.6	29.8 ± 3.9
	13/07/92	0.32	902/50	32.2 ± 2.9	28.1 ± 2.2
	07/06/93	0.14	700/10	28.2 ± 3.7	25.3 ± 1.8
	08/06/93	0.14	710/10	37.0 ± 5.6	33.2 ± 3.6
	07/09/93	0.35	700/10	40.7 ± 6.2	36.6 ± 4.0
T Cep	12/07/92	0.72	700/10	31.0 ± 5.3	27.8 ± 3.6
388	12/07/92	0.72	902/50	28.4 ± 6.5	24.8 ± 5.6
	07/06/93	0.56	833/41	27.6 ± 4.9	23.9 ± 3.5
R Cas	13/07/92	0.05	700/10	34.6 ± 5.4	31.1 ± 3.5
430	13/07/92	0.05	700/10	34.1 ± 5.8	30.6 ± 4.0
	13/07/92	0.05	710/10	45.0 ± 6.9	40.1 ± 4.5
	13/07/92	0.05	710/10	47.8 ± 7.1	42.7 ± 4.5
	13/07/92	0.05	833/41	28.2 ± 4.2	24.5 ± 2.7
	08/06/93	0.82	700/10	36.0 ± 5.6	32.2 ± 3.6
	07/09/93	0.03	700/10	33.5 ± 4.6	30.0 ± 2.5
	08/09/93	0.03	710/10	47.2 ± 6.2	42.1 ± 3.5
	08/09/93	0.03	833/41	29.1 ± 4.8	25.2 ± 3.3

1992; Tuthill et al. 1994a) have followed a two-step procedure that involves fitting a uniform-disc visibility function to their measurements and then applying a 'scaling factor' derived from the models to correct for limb-darkening and atmospheric extension. This was deemed inadequate for our data because, as noted above, a uniform-disc model sometimes produced a poor fit to the observed visibilities. To avoid this problem the model intensity profiles were Fourier transformed and the resulting visibility functions then fitted to the measured data. This gave direct estimates of the photospheric diameters, and furthermore permitted checks to be made on the extent to which the models correctly predicted the observed brightness profiles.

The theoretical brightness distributions were calculated from the spherically extended photospheric models of BSW which are based on the density stratification of non-linear pulsation models covering different phases (and cycles) of three M-type Mira variables. In the absence of separate models tailored for each star in our sample, centre-to-limb brightness profiles were computed for two 'generic' one solar mass Miras. These represented stars pulsating in the fundamental and first-overtone modes; hereafter we shall refer to these as the D and E models respectively. For the D model the underlying non-pulsating AGB star was of luminosity 3470 $L_\odot$ and radius 236 $R_\odot$ and the Mira period was 330 d. For the E model these quantities had values of 6310 $L_\odot$, 366 $R_\odot$, and 328 d. Four centre-to-limb brightness profiles were generated for each model, corresponding to four different phases of the stellar pulsation cycle. These spanned ranges in effective temperature of 2690 – 3050 K for the D model and 2330 – 2760 K for the E model. Because of the variation of $T_{\rm eff}$ with variability phase, and in view of the lack of model atmospheres more closely matched to the individual stars in the sample and the epochs of their observations, we chose to fit the data from each observation with all eight centre-to-limb brightness profiles separately, rather than selecting that profile closest in phase to the observation. This should be a reasonable procedure for near-continuum filters, such as the 830- and 902-nm filters used, for which the shape and extent of the centre-to-limb intensity profiles tended to depend only weakly on the model parameters (Scholz & Takeda 1987; BSW). In this way eight separate estimates for the photospheric diameter of each star were obtained, four based on the hypothesis of fundamental-mode pulsation and four assuming first-overtone pulsation. We have taken the range of each set of four values to be indicative of the uncertainties associated with this model-dependent estimation procedure.

As before, precautions were taken to identify possible departures from circular symmetry prior to model-fitting. For sources showing circularly symmetric visibility functions, models were fitted to azimuthal averages of the Fourier data. However, in cases where the apparent size of the source varied as a function of position angle on the sky, angular 'diameters' were derived by model-fitting to subsets of the visibility data oriented along those position angles at which the source appeared least and most extended. A best-estimate for the photospheric diameter was then computed as the diameter of a sphere having the same volume as the prolate spheroid with major and minor axes as measured. The observed differences between these 'major' and 'minor' axis diameters were as great as 30 per cent in a few instances, particularly for *o* Ceti, χ Cyg, and R Cas at certain epochs.

Results from our model-fitting are given in Table 2, where for each model type (i.e. D or E) we have presented the mean and standard deviation of the diameter estimates obtained from the four time-resolved theoretical brightness profiles. The error estimates include contributions from both the random errors in the visibility measurements and the uncertainties associated with selecting an appropriate model atmosphere. However, as for the analysis in Section 3.1, small systematic effects arising from misfits between the model and measured visibility functions have not been accounted for.

Examination of Tables 1 and 2 shows that the diameter estimates obtained using this more complicated analysis were in general smaller than those inferred from fitting simple uniform-disc models, i.e. at our filter wavelengths the consequences of limb-darkening, which tend to make the star appear smaller in size, were less important than the competing effects due to extension of the stellar atmosphere. This is consistent with modelled and measured spectra of late-type M giants which display substantial molecular band contamination in all optical 'near-continuum' windows bluewards of 1 μm (see e.g. Bessell et al. 1989; Fluks et al. 1994; BSW). It is convenient to characterize the size of a star at a given wavelength in terms of a monochromatic radius, R_λ, which measures the radial coordinate at which $\tau_\lambda = 1$. For any finite bandpass this can be generalized to a filter radius, $R_{\rm f}$, corresponding to the intensity-weighted mean of R_λ over the passband (Scholz & Takeda 1987). For the model atmospheres used in this study, filter radii ranged from $1.18R$ to $1.50R$ for the 700-nm bandpass, from $1.05R$ to $1.36R$ for the 833-nm bandpass, and from $1.03R$ to $1.20R$ for the least blanketed 902-nm bandpass. Hence, observations through all of these filters were expected to show evidence for an extended atmosphere. Typically the $R_{\rm f}/R$ ratios were larger for the low-$T_{\rm eff}$ models ($\leq$ 2760 K: E series, and phase 0.5 of the D series models) and smaller for the high-$T_{\rm eff}$ models ($\geq$ 3030 K: phases 0.8 and 0.0 of the D series models), although a large ratio was also found for the high-$T_{\rm eff}$ (3000 K) phase 0.2 model of the D series.

4 DISCUSSION

4.1 Model atmospheres

Although the primary aim of our study has been to establish the scope of the result of Tuthill et al. (1994a), our monochromatic visibility measurements can also be used to examine the reliability of the atmospheric models of BSW, albeit in a crude fashion.

4.1.1 Variation with radius

One feature of our data that has already been mentioned is the fact that, for stars that were sufficiently resolved, uniform-disc models were unable to reproduce the visibilities measured at the longest baselines. The visibility functions

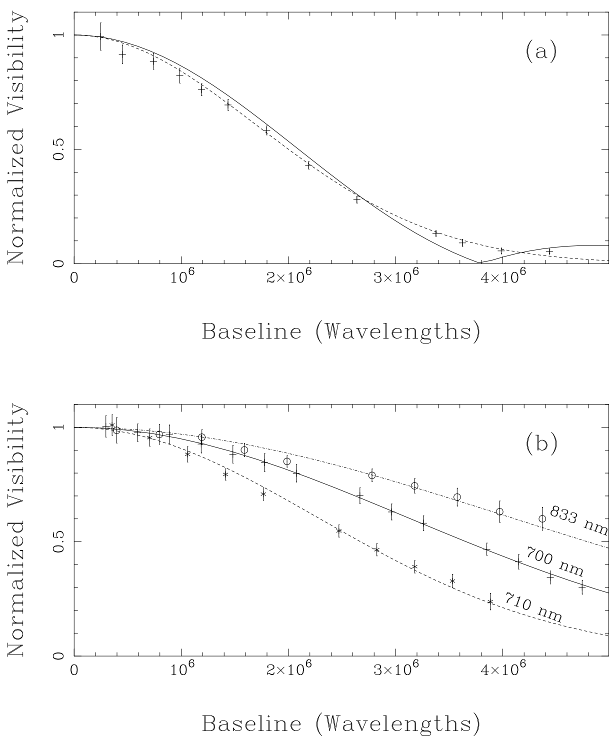

Figure 2. Normalized visibility amplitudes for W Hya (a) and R Cas (b). The first panel shows an azimuthally averaged dataset obtained at 700 nm in 1992 July. The solid line is one of the best-fitting E models, while the dashed line is a Gaussian fit. The second panel shows the variation in visibility of R Cas as a function of wavelength. The data, obtained in 1993 September, have been azimuthally averaged and are shown together with Gaussian fits. The FWHM of the models are 26.7, 34.4, and 20.3 mas at 700, 710 and 833 nm.

predicted on the basis of the theoretical limb-darkened profiles suffered from a similar shortcoming and exhibited sidelobes that were not consistent with our interferometric measurements. An example of this is shown in Fig. 2(a) where it is clear that there is little evidence for a minimum and subsequent rise in the visibility function of W Hya at large baselines. Only a minority of the sources observed were sufficiently resolved so as to permit unambiguous distinction between the Gaussian and limb-darkened models, and so we have been unable to identify any specific features of the model brightness profiles that require modification. Nevertheless, the fact that a misfit was observed in some cases highlights one potential source of uncertainty in our analysis. For fully limb-darkened stars, it is well established that size estimates derived by fitting uniform-disc models can be in error by as much as 13 per cent. However, because of our use of more realistic model brightness profiles, it is probable that the magnitude of this type of systematic error will have been much smaller than this.

Observations at 700 and 710 nm, where the stellar atmosphere often appeared extended (see Tables 1 and 2), were particularly prone to this type of misfit. Because of the strong TiO bandhead close to these wavelengths and the consequent difficulties of correctly modelling the molecular and atomic opacity, it is likely that the model atmospheres we have utilized to correct our raw diameter measurements provide only limited predictive capabilities in this region of the spectrum (see the discussion of BSW). Given these shortcomings it is perhaps not surprising that our data provide evidence for a more extended and gradual drop in brightness away from the centre of the star than predicted. Another possible limitation relates to the observed asymmetries in the stellar brightness distributions. It is now well established that many Mira variables exhibit non-circular morphologies (Karovska et al. 1991; Haniff et al. 1992; Quirrenbach et al. 1992; Wilson et al. 1992; Tuthill et al. 1994b), a feature not yet incorporated into models of stellar atmospheres. In a few cases our data also suggest the presence of localized unresolved hotspots of emission. The existence of such features would be expected to suppress nulls in the observed visibility functions, and this, together with scattering from a circumstellar envelope, would go some way towards explaining the better fit of a Gaussian model to the visibility data of Fig. 2(a).

4.1.2 Variation with wavelength

One of the most useful diagnostics for determining the atmospheric structure of long-period variables is the variation of their monochromatic diameters with wavelength. Detailed modelling (Scholz & Takeda 1987; Bessell et al. 1989) has shown that very large excursions in apparent monochromatic diameter can occur, particularly when crossing regions in the spectrum where the opacity changes rapidly. The models of BSW used here predict somewhat less extreme variations, though the expected ratio of the monochromatic diameter to the photospheric diameter in the strongest TiO bandheads can still approach a factor of two.

Our observations sometimes uncovered variations in apparent angular diameter of more than 50 per cent between different colours at any given epoch. An example of such behaviour is shown in Fig. 2(b), where in 1993 September the ratio of apparent diameters of R Cas at 833 and 710 nm was 0.61. These dramatic changes in size were almost always associated with measurements made at either 700 or 710 nm, at which wavelengths the sources invariably appeared larger than at either 833 or 902 nm. This is consistent with theoretical expectations based on the values of $R_{\rm f}$ which, though not uniquely related to the extension scale of the brightness distribution (Baschek et al. 1991), still provide a sensible measure of it. For the BSW models, values of $R_{\rm f}$ for the 710 nm bandpass were in the range $1.21R - 1.68R$, surprisingly close to those predicted for the 700-nm filter, but larger than the corresponding values for the 830- and 905-nm filter bandpasses (see Section 3.2). The similarity of the values of $R_{\rm f}$ for the 700- and 710-nm filters is indicative of the contribution of the medium-layer photons, which leak through the 710-nm filter's blue wing where the transmission is small (a few per cent) but the intensity relative to the filter centre is high, and which compete with the near-surface photons from the TiO γ bandhead transmitted at the filter centre.

Table 2 shows that the photospheric diameters deduced from the 700- and 710-nm observations tended to be systematically larger than those derived from measurements in the 833- and 902-nm near-continuum filters. In fact, the ratios of the photospheric diameters as inferred from measurements at different wavelengths were in some cases larger than the corresponding ratios obtained using the raw uniform-disc diameter estimates, indicating insufficient scaling of the 700- and 710-nm measurements for the effects of TiO absorption in the higher atmospheric layers of molecular band formation. By using those sets of observations where contemporaneous measurements were obtained through a range of filters, it was possible to derive empirical scaling factors to convert all of the results in Table 2 to a consistent scale. In the mean, we found no significant difference between photospheric diameters derived from data secured at 902 and 833 nm, indicating that the model atmosphere predictions were in good agreement with the observed variations in apparent diameter at these two wavelengths. At 710 and 700 nm, however, mean multiplicative scaling factors of 0.71 ± 0.07 and 0.88 ± 0.11 were required to bring the photospheric diameter estimates into agreement with their longer wavelength counterparts.

If we assume that the BSW models predict the correct functional form for the centre-to-limb brightness profiles in these TiO features, but have the wrong radial extent, then these figures imply increases in the model-averaged filter radii from about $1.3R$ (700 nm) and $1.5R$ (710 nm) to $1.5R$ and $2.1R$, respectively. This is in accord with BSW who state that their models are too compact to predict the large TiO diameters measured by Labeyrie et al. (1977) and Bonneau et al. (1982). The more primitive exploratory models of Bessell et al. (1989) used by Scholz & Takeda (1987) appear more satisfactory in this regard, but any more specific conclusions than this require a more detailed analysis beyond the scope of this paper. This would have to address such issues as the dependence of the TiO features on specific stellar parameters, for example the variability phase and cycle, and would demand more wavelength-selective measurements than are presented here. The interested reader is referred to the more detailed discussion of BSW.

4.1.3 Variation with phase

In the absence of atmospheric models tailored towards individual sources, and with only sparse coverage over the variability cycles for most of our sample, our data have not permitted a detailed investigation of the modulation of photospheric diameter with pulsation phase. Previous observational studies, based on bolometric photometry, have revealed rather small variations in photospheric size of order ± 5 per cent about a mean value over the cycle (see e.g. Tuthill et al. 1994a). On the other hand, theoretical modelling (Bessell et al. 1989; BSW) suggests variations in the range 10–20 per cent, with overtone pulsators tending to exhibit smaller amplitudes than stars oscillating in the fundamental mode. In view of the current uncertainty as to the magnitude of the expected changes of photospheric diameter with pulsation phase, we felt it prudent not to correct further the values in Table 2 for phase-dependent effects. The reader should note that in our subsequent analysis the lack of such an explicit correction could introduce errors of up to ~ 10 per cent.

Table 3. Mean photospheric diameters for the sample stars as inferred from the full set of multi-wavelength measurements given in Table 2. Two values are quoted for each star based on the use of correction factors derived from either fundamental-mode (D) or first-overtone mode (E) models.

Object	Angular Diameter D model (mas)	Angular Diameter E model (mas)
o Cet	38.0 ± 4.0	33.6 ± 3.5
U Ori	21.3 ± 3.7	18.5 ± 2.6
R Cnc	19.7 ± 3.8	17.9 ± 3.6
R Leo	43.4 ± 3.2	37.4 ± 2.3
R Hya	33.0 ± 4.1	28.7 ± 3.3
W Hya	51.8 ± 7.3	46.2 ± 5.8
R Aql	19.5 ± 4.4	17.5 ± 3.7
χ Cyg	32.8 ± 4.1	28.9 ± 3.0
T Cep	28.2 ± 5.4	24.3 ± 4.4
R Cas	28.6 ± 3.9	24.9 ± 2.9

4.1.4 Summary

Our final best-estimates for the apparent photospheric diameters of the sample stars are given in Table 3. These represent weighted means of the multi-epoch measurements presented in Table 2. Because of the uncertainties associated with modelling the Mira atmospheres in high, TiO band forming layers, measurements at 700 and 710 nm were excluded from the analysis where possible. For the two sources (W Hya and R Aql) for which this could not be done, photospheric diameters estimated from data obtained at 700 and 710 nm were used but only after correction using the empirical scaling factors mentioned in Section 4.1.2. In these cases, we have added an additional error of 10 per cent in quadrature with the estimated random and systematic errors to account for the uncertainties in the scaling factors themselves.

In order to assess the overall reliability of the results presented in Table 3 we can compare these data with other independent estimates for the photospheric diameters of the sample members. Of results in the literature, those least affected by systematic sources of error are likely to be those secured in windows at near-infrared wavelengths between 1 and 2 μm. At these wavelengths the effects of atomic and molecular absorption are less severe than in the visible, and so measurements here yield a clearer view of the underlying photospheric continuum emission. Such measurements exist for two stars: o Ceti and R Leo. The angular diameter of o Ceti has been measured in the infrared K band with the Infrared Michelson Array (Ridgway et al. 1992). The atmospheric models of BSW used in this study suggest that the angular diameter measured in the K band should be close to the Rosseland photospheric diameter, and that any correction factor for atmospheric extension and limb-darkening should be small. Ridgway et al. found a uniform-disc diameter of 36.1 ± 1.4 mas, which compares well with the value of 33.6 ± 3.5 mas from the E model-fit of Table 3 (for reasons explained later, we prefer to use the E rather than the D model fits). Di Giacomo et al. (1991) have presented the results of a near-infrared lunar occultation observation of R Leo performed at 2.16 μm where, again, any correction for limb-darkening or photospheric extension should be insignificant. Their value of 33 ± 1.3 mas is somewhat smaller than our best-estimate of 37.4 ± 2.3 mas. However, they state that least-squares fitting led to uniform-disc diameters in the range 30 to 35 mas and it therefore seems possible that their quoted error estimate is optimistic. The small remaining discrepancy between the two results might be due to an extra uncertainty associated with the stellar pulsation.

In summary we have seen that, despite the lengthy procedure required to convert our quasi-monochromatic diameter measurements into estimates of the true photospheric diameter, independent data taken at wavelengths at which the behaviour of cool stellar atmospheres is better understood are in excellent agreement with our own measurements. While this says much for the quality of the state-of-the-art model atmospheres we have utilized, there are other areas where the models and data show obvious inconsistencies. Observational programmes capitalizing on the current generation of long-baseline interferometers would be well suited to probe the effects of atmospheric extension and limb-darkening where data from single monolithic telescopes are just beginning to reveal discrepancies between the models and data. Similarly, programmes concentrating on measurements at specific wavelengths free from atomic and molecular features would go some way towards establishing the true nature of the dynamical behaviour of the deep photospheric layers. We would strongly encourage combined efforts from both theoreticians and observers in these areas.

4.2 Effective temperatures

Estimates of the mean effective temperatures of the sample stars were derived by combining the angular photospheric diameters given in Table 3 with bolometric fluxes using the relation

$$T_{\rm eff} = 2341 (F_{\rm bol}/\phi^2)^{1/4}, \qquad (1)$$

where $F_{\rm bol}$ is the mean apparent bolometric flux in units of 10^{-8} erg cm^{-2} s^{-1} and ϕ is the apparent angular diameter in mas. For cool stars such as LPVs, where most of the luminosity is emitted at near-infrared wavelengths, a convenient method for calculating bolometric magnitudes is to use a blackbody function to interpolate between photometric measurements in the J, H, K and L bands (Robertson & Feast 1981; Glass & Feast 1982; Feast et al. 1989). Here we have followed a similar procedure but have included additional photometry at 1.04 μm (Lockwood 1971) together with *IRAS* data (Beichman et al. 1988). For most of the sample, mean $JHKL$ magnitudes were taken from the compilation of Catchpole et al. (1979), though for a few of the more northern sources further measurements from the literature were included (Gillett, Low & Stein 1968; Wilson et al. 1972; Dyck, Lockwood & Capps 1974; Kenyon & Gallagher 1983; Heske 1990). Because of the proximity of the sample stars no corrections for interstellar extinction were applied. Similarly, no corrections were made to account for H_2O opacity within the near-infrared bandpasses. The latter omission is likely to have led us to overestimate the bolometric fluxes by ~ 0.1 mag. This is slightly smaller than the errors arising from uncertainties in the mean near-infrared magnitudes due to, for example, uneven sampling of the lightcurves, but should be borne in mind when referring to Table 4.

Table 4. Mean effective temperature estimates for the sample stars. Values of $T_{\rm eff}$ have been derived using equation (1) assuming both fundamental (D) and first-overtone (E) pulsation. As described in the text, the mean bolometric magnitudes and blackbody temperatures ($T_{\rm bb}$) were obtained from fits to optical to far-infrared, and to near-infrared photometry respectively.

Object	$m_{\rm bol}$	$T_{\rm eff}$/K D model	$T_{\rm eff}$/K E model	$T_{\rm bb}$/K
o Cet	0.1 ± 0.2	2630 ± 180	2800 ± 190	2770 ± 190
U Ori	2.2 ± 0.2	2170 ± 210	2320 ± 200	2410 ± 130
R Cnc	2.2 ± 0.1	2250 ± 220	2360 ± 240	2550 ± 70
R Leo	0.5 ± 0.2	2240 ± 130	2420 ± 130	2610 ± 110
R Hya	0.5 ± 0.1	2570 ± 170	2760 ± 170	2680 ± 70
W Hya	-0.1 ± 0.2	2360 ± 200	2500 ± 190	2460 ± 110
R Aql	2.2 ± 0.2	2260 ± 280	2390 ± 280	2550 ± 150
χ Cyg	0.8 ± 0.2	2410 ± 190	2570 ± 180	2190 ± 100
T Cep	1.3 ± 0.2	2320 ± 250	2490 ± 250	2520 ± 120
R Cas	1.1 ± 0.2	2410 ± 200	2580 ± 190	2210 ± 130

To accommodate the wide wavelength range of the infrared photometry, a two-component blackbody fit was used as an interpolation device although a single blackbody gave an adequate computation of the bolometric flux for the majority of the sample. In most instances, fits of a single blackbody to the near-infrared data alone ($\lambda \leq 3.5$ μm) revealed excess mid- and far-infrared emission, presumably originating from a circumstellar shell. The use of a two-component blackbody fit included the re-radiated contribution from this warm dust, but in all but two cases the fraction of the bolometric luminosity attributable to this circumstellar component was less than 10 per cent, and in no case did it exceed 20 per cent. The errors in the mean bolometric magnitudes were estimated to be $\lesssim 0.15$ mag.

Values of $T_{\rm eff}$ evaluated using equation (1) are summarized in Table 4, where for each star effective temperatures have been computed on the basis of both the E- and D-type diameter estimates in Table 3. As an alternative to this procedure, we have also included in Table 4 blackbody temperatures obtained by fitting a single blackbody function to the mean near-infrared fluxes between 1.04 and 3.45 μm. In the past there has been some controversy concerning the use of such near-infrared blackbody temperatures as indicators of $T_{\rm eff}$, with Feast and co-workers (Robertson & Feast 1981; Glass & Feast 1982) arguing for approximate equality between $T_{\rm eff}$ and $T_{\rm bb}$, but Bessell et al. (1989) explaining this as a fortuitous coincidence. More recently BSW have favoured a 1.04–4.00 μm blackbody temperature, similar to our 1.04–3.45 μm fit, as a good measure of $T_{\rm eff}$. Our own estimates show reasonable agreement between $T_{\rm eff}$ and $T_{\rm bb}$, although there is marginal evidence that the blackbody temperatures are somewhat higher than the more direct measurements of $T_{\rm eff}$ derived from the photospheric diameters and bolometric magnitudes.

Although these data are probably too inaccurate to draw any definitive conclusions concerning the effective temperature scale for Miras, the very low effective temperatures inferred under the assumption of fundamental-mode pulsation cast doubt on whether such a hypothesis can be entertained. In particular, where independent and reliable measurements of $T_{\rm eff}$ exist in the literature, they agree well with our results based on first-overtone pulsation. For example, Di Giacomo et al. (1991) derived a value of 2450 K for the effective temperature of R Leonis on the basis of their infrared occultation measurement made in a relatively uncontaminated region of the spectrum. This can be compared with our first-overtone measurement of 2420 ± 130 K. Similarly, the interferometric measurement of o Ceti by Ridgway et al. (1992), when corrected for their error in applying a limb-darkening scaling factor, gives a value for $T_{\rm eff}$ of 2720 K, quite similar to our first-overtone temperature of 2800 ± 190 K. The reader should note though that the values given in Table 4 represent mean values for $T_{\rm eff}$: in any real star or realistic model the effective temperature will be a function of variability phase (mainly due to changes in the stellar luminosity) and this should be borne in mind when comparing measurements taken at different epochs.

4.3 Physical diameters and pulsation models

To investigate the pulsation properties of our sample, and in particular the controversy concerning their mode of pulsation (see e.g. Hughes 1993 for a brief summary), we have converted our apparent photospheric angular diameters into linear measures using distance estimates based on the period–luminosity (PL) relation of Feast et al. (1989):

$$M_K = -3.47 \log P + 1.01 \ . \qquad (2)$$

Here M_K is the absolute K magnitude and P the period in days. Mean apparent K magnitudes were obtained as described in Section 4.2 while periods were taken from Kholopov (1987). The resulting distances and linear photospheric radii are given in Table 5 where the errors on the distance estimates have been computed taking into account the uncertainties in the mean K magnitudes (~ 0.1) and the scatter of the empirical PL relation which introduces an additional uncertainty of 0.13 in the distance modulus (Feast et al. 1989).

For many of the stars in our sample, alternative distance estimates based on, for example, spectral type and luminosity (Rowan-Robinson & Harris 1983; Celis 1984) or mass and luminosity (Wyatt & Cahn 1983) exist. Unfortunately, the results of these different methods can vary by as much as a factor of three. The distances quoted in Table 5 generally lie among the smallest of the literature values, and hence our inferred linear photospheric radii are smaller than would otherwise result from using many of the published distances. For two stars (o Ceti and R Leo) trigonometric parallaxes also exist (Jenkins 1952; Gatewood 1992). Our distance estimates for both of these sources of 110 ± 9 pc are consistent with these more direct estimates which give distances of 77 ± 30 pc and 121 ± 15 pc for o Ceti and R Leo respectively.

Table 5. Distances and linear photospheric radii for the sample stars.

Object	Period (days)	Distance (pc)	Radius/$R_\odot$ D model	Radius/$R_\odot$ E model
o Cet	332	110 ± 9	443 ± 59	392 ± 51
U Ori	368	265 ± 21	606 ± 116	526 ± 85
R Cnc	362	255 ± 20	536 ± 112	487 ± 105
R Leo	310	110 ± 9	515 ± 56	444 ± 45
R Hya	389	125 ± 10	442 ± 65	384 ± 54
W Hya	361	95 ± 8	523 ± 85	467 ± 70
R Aql	284	220 ± 18	459 ± 110	412 ± 93
χ Cyg	408	135 ± 11	471 ± 70	415 ± 54
T Cep	388	180 ± 14	545 ± 113	470 ± 93
R Cas	430	160 ± 13	494 ± 78	430 ± 61

Following Tuthill et al. (1994a) we have characterized the mode of pulsation of the sample members using the pulsation equation:

$$Q = P(M/{\rm M}_\odot)^{1/2}(R/{\rm R}_\odot)^{-3/2} \ , \qquad (3)$$

where P is the period in days, M and R the stellar mass and radius respectively, and Q the pulsation constant. Although P can be determined straightforwardly from photometric observations, and M is reasonably well constrained to be $\sim 1\,{\rm M}_\odot$ for Mira variables with moderate (≤ 400 d) periods (see e.g. Wyatt & Cahn 1983; Wood & Bessell 1983; Feast & Whitelock 1987), previous attempts at using equation (3) directly have foundered because of the difficulties associated with determining accurate stellar radii. As a result, in the past, mode identification has mainly either relied upon photometric estimates of stellar radii (Robertson & Feast 1981; Glass & Feast 1982; Whitelock 1986) or has utilized alternative methods involving the dynamical modelling of shock-front speeds in Mira atmospheres (Hill & Willson 1979; Willson 1983; Tuchman 1991). The results of these studies have remained stubbornly inconclusive, with analyses of the same observational data sometimes giving rise to inconsistent conclusions (see e.g. Wood 1990a; Tuchman 1991). Our approach here has been to use our interferometric estimates of photospheric radii in conjunction with equation (3) to provide estimates for Q which can be directly related to the dynamical states of the stars.

The relationship between period, mass, and radius for fundamental-mode pulsators (cf. equation (3)) can be expressed more precisely in the following form (Wood 1990a):

$$\log(P) = -2.07 + 1.94 \log(R/{\rm R}_\odot) - 0.9 \log(M/{\rm M}_\odot), \qquad (4)$$

where P is measured in days. For first-overtone pulsators we have used the theoretical results of Fox & Wood (1982) to construct a similar relation relating P, M and R. These predictions for fundamental and first-overtone pulsators of various masses are shown graphically in Fig. 3, where we have also plotted our experimentally determined photospheric radii. For the sake of clarity, we have only presented those results obtained after correction for limb-darkening and atmospheric extension using first-overtone model atmospheres (E models). The corresponding D model radii are approximately 15 per cent larger and so will not be considered further here.

It is evident from Fig. 3 that our data rule out fundamental-mode pulsation for the complete sample of 10 Miras, in full support of the earlier result of Tuthill et al. (1994a). Even for masses as high as 1.5 $M_\odot$, which themselves are unlikely given the high mass-loss rates associated with long-period-variables (see e.g. Knapp & Morris 1985), our measurements preclude fundamental-mode pulsation for all but one of the sample. Indeed, it is tempting to conclude that all the sample stars have photospheric radii in the range $400 - 500\,R_\odot$ consistent with the suggestion of Feast et al. (1989) that Miras are a physically well-defined class of object occupying an instability strip of finite width in the HR diagram.

In view of the circuitous route we have taken to arrive at Fig. 3 it is worth reviewing a number of the steps in the development of our argument. Although our quasi-monochromatic diameter estimates are well constrained by the data, the process of converting these to photospheric radii is worthy of examination. Despite the noticeable limitations of the theoretical models used to perform this conversion, it is unlikely that these shortcomings will have contributed to our final result: measurements obtained at those wavelengths at which these limitations were most noticeable (700 and 710 nm) were largely excluded from our analysis. Furthermore, the good agreement between independent measurements obtained in the near-infrared provides strong evidence that the corrections applied for photospheric extension and limb-darkening cannot have been wrong by large factors, and in addition rules out the possibility that some further effect (e.g. dust scattering) might be causing the sources to appear greatly extended. Similarly, errors in our distance estimates are unlikely to be large enough to affect our conclusions. Whilst modifications to equation (2) at the 10 per cent level have previously been suggested to account for metallicity effects (Wood 1990a), a recent re-evaluation (Whitelock et al. 1994) of the PL relations for both local and LMC Miras does not support this claim and is fully consistent with the relation adopted here. The close agreement between the PL distance and the directly determined trigonometric parallax distance of R Leo (Gatewood 1992) further supports this conclusion.

Perhaps the most uncertain stage in our analysis concerns the assumed masses of Mira variables. It is generally accepted that the main-sequence progenitors of Miras are $\lesssim 2$-$M_\odot$ stars, with those heavier than this evolving through the AGB without penetrating the instability region occupied by Miras (Wood & Cahn 1977; Cahn & Wyatt 1978). The theoretical models, on which these conclusions are based, have been used by Wyatt & Cahn (1983) to derive the main-sequence masses of nine of our sample members: all were found to lie between 1 and 1.35 $M_\odot$. Note that the stars are likely to be substantially lighter than this now because of their individual mass-loss histories. Unfortunately, observational verification of these theoretical results has been problematic. One approach has been to identify Miras in binary systems. Although a handful of these are known, very few instances of direct determinations of their masses have been made. Fernie (1959) used visual orbit information together

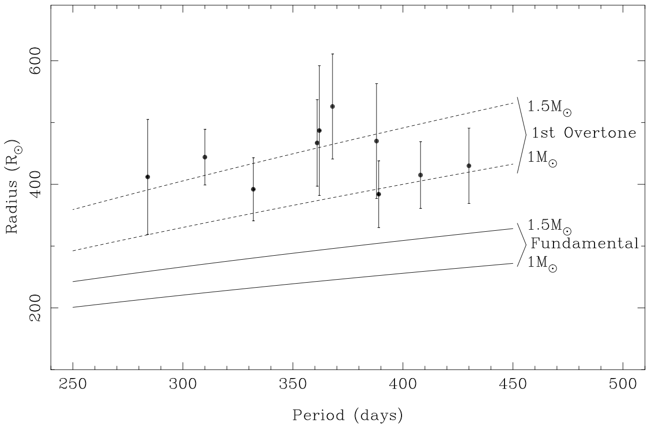

Figure 3. Stellar radius versus pulsation period for the 10 Miras in our sample. The radii plotted correspond to those corrected using the E model atmospheres mentioned in the text. Values for the photospheric radii corrected using the D model atmospheres were approximately 15 per cent larger. The lines denote theoretical predictions for 1- and 1.5-$M_\odot$ stars pulsating in the fundamental and first-overtone modes.

with velocity data to estimate the mass of X Oph as 1 $M_\odot$, but, since his data covered only one-tenth of an orbital cycle, this value is probably not accurate to better than a factor of two. Analyses based on the empirical PL relation, the somewhat uncertain effective temperature scale for Miras, and theoretical predictions of the pulsation constant have generally argued for pulsation masses $\lesssim 1.5$ $M_\odot$ for Miras with periods of up to 400 d (Wood & Bessell 1983; Wood, Bessell & Fox 1983; Feast & Whitelock 1987). This is consistent with studies of short-period (200–300 d) Miras in metal-rich globular clusters which should have masses somewhat less than 1 $M_\odot$ (see e.g. Whitelock 1986). Given the individual uncertainties associated with each of these methods, further and more precise mass determinations would clearly be preferred. However, while masses as large as 2 $M_\odot$ cannot be excluded for our sample stars, most of the evidence points towards lower values.

Notwithstanding these concerns, it seems unlikely that Miras with periods in the range 280 to 430 d can be pulsating in the fundamental mode without invoking either an upward revision of their mass scale or a re-interpretation of their PL relations. Our conclusion is consistent with many earlier empirical and indirect studies (see e.g. Wood 1975; Robertson & Feast 1981; Glass & Feast 1982; Whitelock 1986; Balmforth, Gough & Merryfield 1990; Perl & Tuchman 1990; Barthès & Tuchman 1994) but still leaves a number of important questions unresolved. Of particular interest is the discrepancy between the observed and predicted shock-front velocities for overtone pulsators (see e.g. Wood 1990b for a discussion of these issues) and the possibility that the stars in our sample may be pulsating in higher (e.g. second) overtone modes. In addition to predicting overtone pulsation in Miras with periods greater than 150 d, Robertson & Feast (1981) have suggested that those with shorter periods are anomalous and may be fundamental pulsators. High-precision parallax measurements from the *Hipparcos* mission, together with monochromatic near-infrared angular diameter measurements using the 10-m class telescopes now coming on-line, should soon provide the necessary data to address these questions directly.

5 CONCLUSIONS

We have used new high-precision monochromatic angular diameter measurements in conjunction with dynamical models of cool stellar atmospheres to investigate the pulsational properties of a sample of 10 Mira variables. Our data suggest that none of the sample, which includes stars with periods ranging from 284 to 430 d, pulsates in the fundamental mode, confirming an earlier result for R Leonis (Tuthill et al. 1994a). For fundamental-mode pulsation to be consistent with our measurements would require revision of either the PL relation or the mass scale for Miras, both of which are unlikely. Our observations have demonstrated the diagnostic capabilities of optical interferometric observations in testing the predictive capacity of state-of-the-art cool model atmospheres. The forthcoming availability of high-precision parallaxes from the *Hipparcos* satellite means that further such observations, in specific near-infrared bandpasses and with large 10-m class telescopes (both monolithic and separated-element), offer the possibility of extending our result both to larger samples and to Miras with shorter ($\leq$ 250 d) and/or longer ($\geq$ 450 d) periods in the very near future.

ACKNOWLEDGMENTS

It is a pleasure to thank Peter Wood, Michael Feast and John Baldwin for their comments and continued interest, and Franz Kerschbaum for his spectral energy distribution fitting software. We are grateful to the American Association of Variable Star Observers and the British Astronomical Association (Variable Star Section) for their assistance, and to the many members of our group and staff at the WHT (in particular Richard Wilson) without whom the observations reported here would not have been possible. Financial support from the Royal Society (CAH), the Cambridge Commonwealth Trust and the Cambridge Philosophical Society (PGT) are gratefully acknowledged. The William Herschel Telescope is operated on the island of La Palma by the Royal Greenwich Observatory in the Spanish Observatorio del Roque de los Muchachos of the Instituto de Astrofísica de Canarias.

REFERENCES

Balmforth N.J., Gough D.O., Merryfield W.J., 1990, in Mennessier M.O., Omont A., eds, From Miras to Planetary Nebulae: Which Path for Stellar Evolution? Editions Frontières, Gif-sur-Yvette, p. 85
Barthès D., Tuchman Y., 1994, A&A, 289, 429
Baschek B., Scholz M., Wehrse R., 1991, A&A, 246, 374
Beach T.E., Willson L.A., Bowen H.G., 1988, ApJ, 329, 241
Beichman C.A., Neugebauer G., Habing H.J., Clegg P.E., Chester T.J., 1988, Infrared Astronomical Satellite Catalogs and Atlases, Vol 2-6. NASA RP-1190, Washington D.C.
Bessell M.S., Scholz M., 1989, in Johnson H.R., Zuckerman B., eds, Proc. IAU Colloq. 106, Evolution of Peculiar Red Giant Stars. Cambridge University Press, Cambridge, p. 67
Bessell M.S., Brett J.M., Scholz M., Wood P.R., 1989, A&A, 213, 209
Bessell M.S., Scholz M., Wood P.R., 1995, A&A, submitted (BSW)
Bonneau D., Foy R., Blazit A., Labeyrie A., 1982, A&A, 106, 235
Buscher D.F., Haniff C.A., Baldwin J.E., Warner P.J., 1990, MNRAS, 245, 7P
Cahn J.H., Wyatt S.P., 1978, ApJ, 221, 163
Catchpole R.M., Robertson B.S.C., Lloyd Evans T.H.H., Feast M.W., Glass I.S., Carter B.S., 1979, S. Afr. Astron. Obs., Circ., 4, 61
Celis L.S., 1984, AJ, 89, 1343
Di Giacomo A., Richichi A., Lisi F., Calamai G., 1991, A&A, 249, 397
Dyck H.M., Lockwood G.W., Capps R.W., 1974, ApJ, 189, 89
Feast M.W., Whitelock P.A., 1987, in Kwok S., Pottasch S.R., eds, Late Stages of Stellar Evolution. Reidel, Dordrecht, p. 33
Feast M.W., Glass I.S., Whitelock P.A., Catchpole R.M., 1989, MNRAS, 241, 375
Fernie J.D., 1959, ApJ, 130, 611
Fluks M.A., Plez B., Thé P.S., de Winter D., Westerlund B.E., Steenman H.C., 1994, A&AS, 105, 311
Fox M.W., Wood P.R., 1982, ApJ, 259, 198
Gatewood G., 1992, PASP, 104, 23
Gillett F.C., Low F.J., Stein W.A., 1968, ApJ, 154, 677
Glass I.S., Feast M.W., 1982, MNRAS, 199, 245
Habing H.J., 1990, in Mennessier M.O., Omont A., eds, From Miras to Planetary Nebulae: Which Path for Stellar Evolution? Editions Frontières, Gif-sur-Yvette, p. 16
Haniff C.A., Buscher D.F., 1992, J. Opt. Soc. Am. A, 9, 203
Haniff C.A., Mackay C.D., Titterington D.J., Sivia D., Baldwin J.E., Warner P.J., 1987, Nat, 328, 694
Haniff C.A., Ghez A.M., Gorham P.W., Kulkarni S.R., Matthews K., Neugebauer G., 1992, AJ, 103, 1662
Heske A., 1990, A&A, 229, 494
Hill S.J., Willson L.A., 1979, ApJ, 229, 1029
Hughes S.M.G., 1993, in Nemec J., ed., Proc. IAU Colloq. 139, New Perspectives on Stellar Pulsations and Pulsating Variable Stars. Kluwer, Dordrecht, p. 192
Jenkins L.F., 1952, General Catalogue of Trigonometric Stellar Parallaxes. Yale University Press, New Haven
Karovska M., Nisenson P., Papaliolios C., 1991, ApJ, 374, L51
Kenyon S.J., Gallagher J.S., 1983, AJ, 88, 666
Kholopov P.N., 1987, General Catalogue of Variable Stars, Fourth Edition. Nakua Publ. House, Moscow
Knapp G.R., Morris M., 1985, ApJ, 292, 640
Labeyrie A., Koechlin L., Bonneau D., Blazit A., Foy R., 1977, ApJ, 218, L75
Lockwood G.W., 1971, ApJ, 169, 63
Nakajima T., Kulkarni S.R., Gorham P.W., Ghez A.M., Neugebauer G., Oke J.B., Prince T.A., Readhead A.C.S., 1989, AJ, 97, 1510
Perl M., Tuchman Y., 1990, ApJ, 360, 554
Quirrenbach A., Mozurkewich D., Armstrong J.T., Johnston K.J., Colavita M.M., Shao M., 1992, A&A, 259, L19
Ridgway S.T., Benson J.A., Dyck H.M., Townsley L.K., Hermann R.A., 1992, AJ, 104, 2224
Robertson B.S.C., Feast M.W., 1981, MNRAS, 196, 111
Roddier F., 1988, Phys. Rep., 170, 97
Rowan-Robinson M., Harris S., 1983, MNRAS, 202, 767
Scholz M., 1992, A&A, 253, 203
Scholz M., 1993, in Nemec J., ed., Proc. IAU Colloq. 139, New Perspectives on Stellar Pulsations and Pulsating Variable

Stars. Kluwer, Dordrecht, p. 201
Scholz M., Takeda Y., 1987, A&A, 186, 200 (erratum: A&A, 196, 342
Tuchman Y., 1991, ApJ, 383, 779
Tuthill P.G., Haniff C.A., Baldwin J.E., Feast M.W., 1994a, MNRAS, 266, 745
Tuthill P.G., Haniff C.A., Baldwin J.E., 1994b, in Robertson J.G., Tango W.J., eds, Proc. IAU Symp. 158, Very High Angular Resolution Imaging. Kluwer, Dordrecht, p. 395
Whitelock P.A., 1986, MNRAS, 219, 525
Whitelock P.A., Menzies J., Feast M., Marang F., Carter B., Roberts G., Catchpole R., Chapman J., 1994, MNRAS, 267, 711
Willson L.A., 1983, in Cox J.P., Hansen C.J., eds, Pulsations in Classical and Cataclysmic Variable Stars. University of Colorado, Boulder, p. 284
Wilson R.W., Baldwin J.E., Buscher D.F., Warner P.J., 1992, MNRAS, 257, 369
Wilson W.J., Schwartz P.R., Neugebauer G., Harvey P.M., Becklin E.E., 1972, ApJ, 177, 523
Wood P.R., 1975, MNRAS, 171, 15P
Wood P.R., 1990a, in Mennessier M.O., Omont A., eds, From Miras to Planetary Nebulae: Which Path for Stellar Evolution? Editions Frontières, Gif-sur-Yvette, p. 67
Wood P.R., 1990b, in Cacciari C., Clementini G., eds, ASP Conf. Series Vol. 11, Confrontation between Stellar Pulsation and Evolution. Astron. Soc. Pac., San Fransisco, p. 355
Wood P.R., Bessell M.S., 1983, ApJ, 265, 748
Wood P.R., Cahn J.H., 1977, ApJ, 211, 499
Wood P.R., Bessell M.S., Fox M.W., 1983, ApJ, 272, 99
Wyatt S.P., Cahn J.H., 1983, ApJ, 275, 225

This paper has been produced using the Blackwell Scientific publications LaTeX style file.